Sains Malaysiana 46(7)(2017): 1025–1031
http://dx.doi.org/10.17576/jsm-2017-4607-03

The Effect of Graphene Content on the Structure and Conductivity of Cellulose/Graphene Composite

(Kesan Kandungan Grafin terhadap Struktur dan Kekonduksian Komposit Selulosa/Grafin)

FARZANA ABD HAMID, FAUZANI MD SALLEH*, NOR SABIRIN MOHAMED & SYED BAHARI RAMADZAN SYED ADNAN

ABSTRACT

The effect of graphene content on the structure and conductivity of an eco-friendly cellulose/ graphene (CG) composite was investigated. Different compositions of graphene content from 0 to 70 wt. % were prepared using the sol-gel method. Ionic liquids 1-butyl-3-methyl-imidazolium chloride was used to disperse graphene between the cellulose. The investigation showed that CG composite with higher graphene composition exhibits higher conductivity. The highest conductivity (2.85×10^{-4} S cm^{-1}) was observed at 60 wt. % graphene composition. Sample without graphene showed the lowest conductivity of 1.77×10^{-7} S cm^{-1}, which acts as an insulator. The high conductivity of CG composite can be associated with the X-ray diffraction (XRD) patterns. The XRD patterns of α-cellulose exhibits a decrease in crystallinity at peak 15° and 22° due to the depolymerization in CG composite. At 60 wt. % composition, XRD pattern showed the decrease in intensity at peak 26° indicates that graphene is more dispersed in the cellulose mixture. This is supported by Fourier transform infrared spectrum of CG composite where the absorption peaks of C-O stretching are weakened at wavelength of 1163 and 1032 cm^{-1}, suggested dehydration and rupture of cellulose. The dehydration and rupture of cellulose result in the high conductivity of CG composite. This research is believed to provide an eco-friendly method to produce cellulose/graphene composite which is useful in future applications of energy.

Keywords: Cellulose/graphene composite; conductivity; ionic liquid; XRD pattern

ABSTRAK

Kesan kandungan grafin terhadap struktur dan kekonduksian komposit selulosa/grafin (CG) mesra alam telah dikaji. Komposisi berbeza kandungan grafin daripada 0 kepada 70 % bt. telah disediakan melalui kaedah sol-gel. Cecair ionik 1-butil-3-metil-imidazolium klorida telah digunakan untuk menyebarkan grafin antara selulosa. Kajian menunjukkan bahawa komposit CG dengan komposisi grafin yang lebih tinggi mempamerkan kekonduksian lebih tinggi. Kekonduksian tertinggi (2.85×10^{-4} S cm^{-1}) diperhatikan pada komposisi 60 % bt. grafin. Sampel tanpa grafin menunjukkan kekonduksian terendah 1.77×10^{-7} S cm^{-1} yang bertindak sebagai penebat. Kekonduksian tinggi komposit CG boleh dikaitkan dengan corak pembelauan sinar-X (XRD). Corak XRD α-selulosa menunjukkan penurunan penghabluran pada puncak 15° dan 22° yang mungkin disebabkan oleh penceraian polimer pada komposit CG. Pada komposisi 60 % bt., corak XRD menunjukkan penurunan dalam keamatan di puncak 26° yang menunjukkan bahawa grafin lebih tersebar dalam campuran selulosa. Ini disokong oleh spektrum inframerah transformasi Fourier (FTIR) komposit CG, dengan puncak penyerapan regangan C-O menjadi lemah pada panjang gelombang 1163 dan 1032 cm^{-1}, mencadangkan berlakunya dehidrasi dan perpecahan di dalam selulosa. Hal ini menyebabkan kekonduksian yang tinggi pada komposit CG. Kajian ini dipercayai untuk menyediakan satu kaedah yang mesra alam bagi menghasilan komposit selulosa/grafin yang berguna dalam aplikasi tenaga pada masa hadapan.

Kata kunci: Cecair ionik; corak XRD; kekonduksian; komposit selulosa/grafin

INTRODUCTION

Solid electrolyte has emerged as an active research field replacing liquid electrolyte. Its numerous advantages such as safe and no electrolyte leakage, high-energy storage capacity, good cyclability, have a flexible geometry, can be processed easily and great mechanical strength would overcome the limitations in the liquid electrolyte.

Graphene has a two dimensional structure, the carbon atoms arranged in hexagonal lattice due to their sp^2 hybridization. It has exceptional electronic properties such as very conductivity (Castro Neto et al. 2009), high specific area (Xu et al. 2015), great thermal and mechanical properties (Changgu et al. 2008; Hossain et al. 2014). Graphene also widely used in fuel cells (Mahmood et al. 2014), as corrosion prevention (Li et al. 2016), ultraviolet photo-detector (Zhang et al. 2016), chemical and biological sensor (Zhao et al. 2016) and main component of cathode in lithium ion batteries (Patel et al. 2014).

An extensive study on cellulose has been done for the past few decades due to its eco-friendly properties. Cellulose is not melt able, insoluble in water or common solvents making it difficult to be derived or utilize. Cellulose hydrogel or cellulose composite was discovered and applied in various research fields such as food (Lavoinea et al. 2016), sensing (Sadasivuni et al. 2016) and tissue engineering (Singh et al. 2016; Xu et al. 2015). Cellulose film was fabricated using ionic liquid as solvent then plasticizer was added to improve its physical properties (Pang et al. 2013).

Ionic liquid is widely used as a solvent to dissolve the cellulose due to its environmental friendly properties (Soheilmoghaddam et al. 2014). It has exceptional characteristics such as high thermal and electrochemical stability, non-flammability and low vapor pressure. Due to its versatility, ionic liquids are used in various applications such as batteries (Safa et al. 2016), super-capacitors (Bag et al. 2016), lubricants (Qu et al. 2016) and biodiesel production (Troter et al. 2016).

There are number of studies on cellulose/graphene composite focusing on its physical properties. Xu et al. (2015) prepared cellulose/graphene composite from ionic liquid (IL) solution using deionized water as coagulant. Improvement in properties of cellulose was shown by adding graphene into cellulose-ionic liquid. Mechanical and thermal properties of modified cellulose by reduced graphene oxide (rGO) increased compared to the pure cellulose hydrogels. This is due to the presence of 3D network structure and graphene nanosheets were uniformly dispersed within the hydrogels. Feng et al. (2012), made a conductive, flexible and mechanically strong cellulose/graphene nanocomposite film using vacuum-assisted-self-assembly technique. Increase in mechanical strength is the result of oxygen content in graphene oxide (GO) interacted with bacterial cellulose (BC) via hydrogen bonding which promotes stress transfer between GO and BC. Tian et al. (2014) carried out and experiment on regenerated cellulose/graphene (RC/G) composite by applying wet spinning method. The tensile strength of regenerated cellulose/graphene increased with increasing graphene loading due to homogeneous graphene dispersion. Increased in graphene loadings also showed enhancement in thermal conductivity up to 30% where less heat needed for temperature rising. Based on the literature review, there is no previous study on CG composite as solid electrolyte is done.

In the present study, CG composite solid electrolyte was successfully synthesized. Ionic liquid BmimCl was used to dissolve α-cellulose and capable to disperse graphene. Different composition of cellulose/graphene was varied to study the effect of graphene content on the structure and conductivity of eco-friendly CG composite solid electrolyte.

Materials and Methods

Black color granulated graphene was supplied by Chemolab Supplies, Malaysia. It has a density of 0.3 g/cm^3 with average diameter of 5 mm and 99.5% carbon content. Granulated graphene was ground to form powder before being used for experimental purpose. A white color of α-cellulose powder with a bulk density of 3.1-4.3 (CC/g) was obtained from Sigma-Aldrich Co. (St. Louis, USA). A pale yellow color BmimCl ionic liquid was purchased from Merk (Darmstadt, Germany). Molecular formula of BmimCl is $C_8H_{15}ClN_2$ and molar mass of 174.68 g/mol. The melting point of BmimCl is 60ºC and it is a hygroscopic material.

Graphene dispersion was prepared by dissolving graphene powder in BmimCl using ultrasonic treatment at 80ºC for 6 h. α-cellulose powder was also dissolved in BmimCl and heated in oil bath at 110ºC for 1 h. Then, graphene dispersion was poured into α-cellulose solution. The mixture undergoes magnetic stirring for 30 min at 110°C. It was then casted in a petri dish and let dry at room temperature for 3 days. CG composite obtained was kept in a desiccator for 1 day before being further analyzed. Different composition of cellulose/graphene samples were prepared and labeled as CG-0, CG-1, CG-2, CG-3, CG-4, CG-5, CG-6 and CG-7 are listed in Table 1. Graphene composition is limited up to 70 wt. % as composition greater than this value produced unstable film.

TABLE 1. Composition of cellulose/ graphene composite

Ratio of cellulose/graphene composite	Label
10:0	CG-0
9:1	CG-1
8:2	CG-2
7:3	CG-3
6:4	CG-4
5:5	CG-5
4:6	CG-6
3:7	CG-7

Changes in functional groups were detected using Fourier Transform Infrared (FTIR) by Perkin Elmer Frontier with Attenuated Total Reflectance (ATR) sampling technique. The resolution used was 2 cm^{-1} in the wavelength range from 550 to 4000 cm^{-1}. XRD patterns were studied using D8 Advance X-ray Diffraction-Buker AXS with Cu K_α radiation ($\lambda = 0.15418$ nm) in the light scattering range of 5° - 90° (2θ) at room temperature. Conductivity of samples were investigated using Solartron 1260 Impedance analyzer in the frequency range from 1 MHz to 10 Hz at room temperature with applied voltage of 100 mV.

Results and Discussion

FTIR ANALYSIS

IR spectra shown in Figure 1 consist of BmimCl, graphene, α-cellulose, CG-0 and CG-6. Intense absorption at 1568 and 3055 cm^{-1} in the IR spectrum of BmimCl

(Figure 1(b)) indicated the C=C and sp^2 =CH stretching, respectively, which referred to the aromatic compound. The hydroxyl peak (-OH) of water in BmimCl was observed at 3375 cm^{-1}. There were absorptions of methyl sp^3(-CH_3) stretching vibrations of the asymmetric (ν_{as}) at 2957 cm^{-1} and the symmetric (ν_s) at 2871 cm^{-1} in BmimCl. High intensity peak at 1168 cm^{-1} in BmimCl is attributed to in-plane C-H bending of aromatic compound while a sharp peak at 752 cm^{-1} represents C-Cl stretching vibration of alkyl halides in BmimCl.

IR spectrum of pure α-cellulose (Figure 1(b)) exhibited broad peak at 3324 cm^{-1} corresponding to -O-H stretching vibration of hydroxyl group. Slight peak absorption was observed at 2865 cm^{-1} was attributed to C-H stretching vibration. The peaks observed at 1161 and 1018 cm^{-1} were attributed to C-O stretching vibration.

Figure 1(a) shows the IR spectrum of CG composite at 0 wt. % (CG-0) and 60 wt. % graphene loading (CG-6). The hydroxyl peak absorption (-OH) of α-cellulose was compared with CG composite (CG-0 and CG-6). From Figure 1, the hydroxyl peak of α-cellulose was observed at 3324 cm^{-1}. This peak was found shifted to 3356 cm^{-1} in CG-0 and CG, indicates reaction that caused fracture of hydrogen bonds (Ye et al. 2016).

It was also discovered that C-H stretching peak also shifted to 2874 cm^{-1} in the CG-0 and CG-6 compared to the one in α-cellulose (2865 cm^{-1}). The presence of new peak absorptions observed at 2960 and 2933 cm^{-1} in CG-0 and CG-6, respectively, are traces of C-H stretching vibration from the reaction of BmimCl and α-cellulose. CG-6 demonstrated weaker absorption at 2960, 2933, 2874, 1163 and 1032 cm^{-1} due to the amount of cellulose ratio is completely reduced along with dehydration and rupture of α-cellulose (Ye et al. 2016). Traces of C=C stretching vibration of aromatic compound from BmimCl were shown in the CG-0 and CG-6 composites at 1568 and 1566 cm^{-1}, respectively. A slight peak absorption at 750 cm^{-1} in CG-0 and CG-6 corresponding to C-Cl stretching vibration of alkyl halides resulted from traces of BmimCl.

XRD ANALYSIS

Figure 2(a) and 2(b) shows the XRD pattern of graphene and α-cellulose & ionic liquid, respectively. In Figure 2(a), a sharp peak appeared at 26° (002) for pure graphene indicate high crystallinity. From Figure 2(b) α-cellulose peaks were exhibited peak at 15° and 22° referred to the semi crystalline properties of the material. An indistinct peak of BmimCl at 23° might reflect the amorphous structure of BmimCl. The decrease in degree crystallinity of graphene was shown in Figure 2(c) and 2(d) where the peak intensity of graphene in CG composite at 26° (002) was significantly reduced due to ultra-sonication (Ye et al. 2016). The reduction in crystallinity also suggests that graphene is dispersed in α-cellulose medium (Feng et al. 2012). BmimCl has moderate dielectric constant

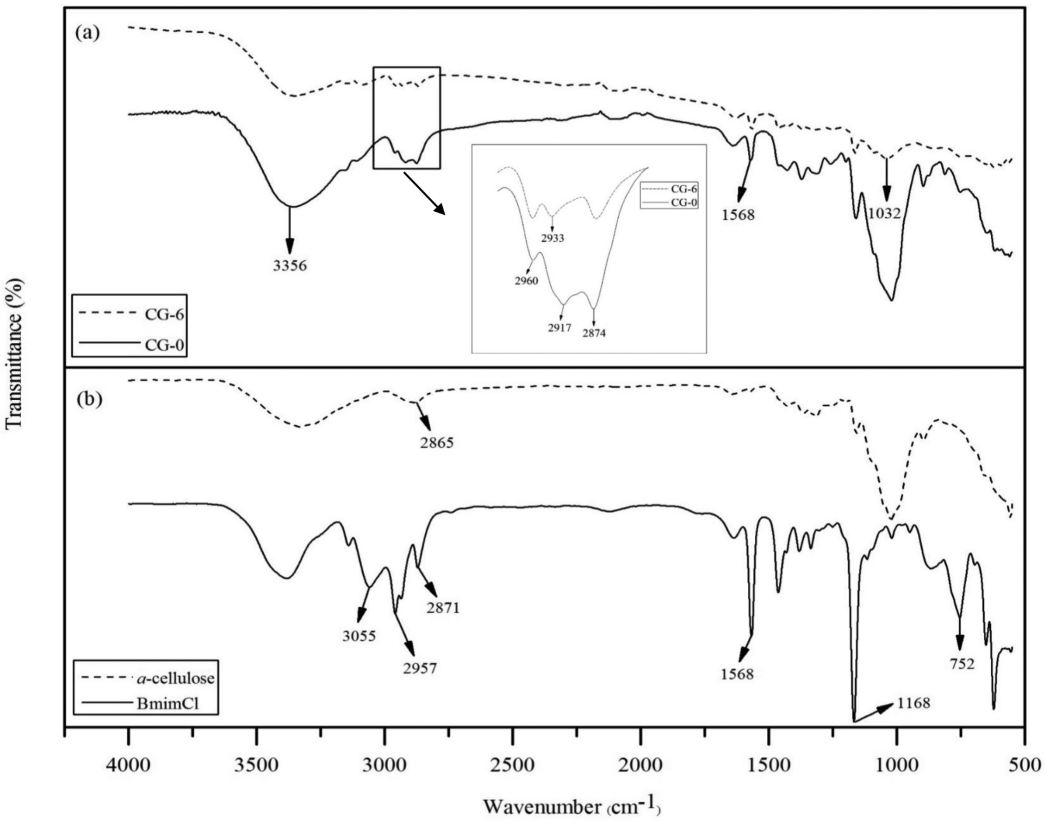

FIGURE 1. FTIR spectrum of (a) CG-6 & CG-0 and (b) α-cellulose & BmimCl

which provides shielding for stacking interaction between graphene sheets. This van der Waals interaction leads to graphene dispersion (Xu et al. 2015).

Figure 2(c) and 2(d) present the XRD patterns of CG composites, both figures shows a high intensity at peak 47° and low intensity peak at 76°. The formation of new crystalline phase is due to interaction between α-cellulose and BmimCl. The interaction is expected to form C-H bond. This is supported by IR spectrum in Figure 1, where initial peak absorption at 3055, 2957 and 2871 cm^{-1} for BmimCl and 2865 cm^{-1} for α-cellulose which associated to C-H stretching vibrations shifted to 2960, 2933 and 2874 cm^{-1} in CG composites. In Figure 2(c), the peak intensity at 47° for CG-0 and CG-6 are 488 and 340 a.u., respectively. Greater peak intensity in CG-0 may be related with the changes in IR spectrum where the band absorption at 2960, 2933 and 2874 cm^{-1} for CG-0 is slightly stronger compared to CG-6. However, greater peak intensity at 47° was discovered for CG-3 and CG-4 which are 671 and 566 a.u., respectively. The low peak intensity at 47° for CG-6 is because graphene added disturbed the interaction between α-cellulose and BmimCl thus resulting in increase in amorphous region which enhanced the movement of electrons leading to higher conductivity.

It was found that CG-6 exhibits almost smooth line at 15° and 22° when XRD pattern of α-cellulose was compared with CG-6, indicates the depolymerization of α-cellulose resulted from increased in amorphous phase. The present of BmimCl in the CG composites decreased the crystallinity of α-cellulose effectively by forming new hydrogen bonds with α-cellulose and then break the hydrogen bond. The forming and breaking of hydrogen bond leads to cleavage of lignin-hemicellulose linkages (Bhaumik & Dhepe 2015).

EFFECT OF GRAPHENE CONTENT ON CONDUCTIVITY OF CG COMPOSITE

Figure 3 shows conductivity of CG composite with different graphene compositions. The highest conductivity

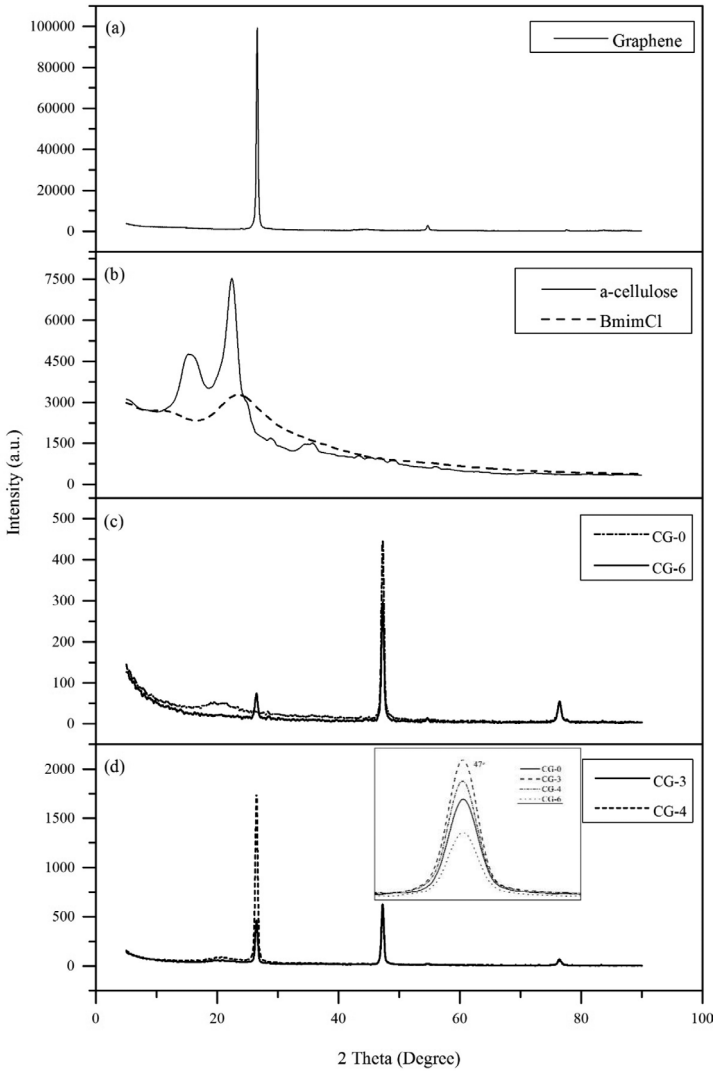

FIGURE 2. XRD patterns of (a) pure graphene, (b) α-cellulose & BmimCl, (c) CG-0 & CG-6 and (d) CG-3 & CG-4

is demonstrated by CG-6 with conductivity of 2.85× 10^{-4} S cm^{-1}. The highest conductivity obtained from this research is lower compared to the conductivity of bacterial cellulose/graphene nanocomposite (1.1× 10^{-2} S cm^{-1}) conducted by Feng et al. (2012). However, the bacterial cellulose/graphene nanocomposites were made up of bacterial cellulose which are not long lasting. CG composites produced in this research are more stable and more suitable for longer shelf life. The lowest conductivity of CG composite is shown by CG-0 with conductivity 1.77×10^{-7} S cm^{-1} which acts as an insulator. The addition of graphene into the CG composite seems to improve the conductivity of the composite. Figure 4(a) and 4(b) displays Nyquist plot of CG-0 and CG-6, respectively. Boundary resistance for CG-0 insulator is 1.97×10^5 Ohm while CG-6 has the lowest boundary resistance of 124.87 Ohm. Spikes in Figure 4(b) indicates charge across electrode/electrolyte (E/E) at inter-face, while large semicircle curve in Figure 4(a) represents the nature of E/E interfaces that caused greater double layer effect. The highest conductivity of CG-6 could be related to the XRD pattern in Figure 2(c) where at 60 wt. % graphene loading, XRD pattern displayed lowest graphene intensity suggesting uniform graphene dispersion causing conductive network formation in the composite (Feng et al. 2012). XRD patterns of CG-3 and CG-4 in Figure 2(d) shows increased in crystallinity. The abnormal conductivity patterns in CG-3 and CG-4 (Figure 3) can be explained from increased crystallinity peak of XRD shown in Figure 2(d). The decreased in the conductivity of CG-3 and CG-4 composites were related to the increased in crystallinity caused by largely undispersed graphene component in the CG composite. As discussed before, XRD pattern of CG-6 is compared with α-cellulose and it was discovered that CG-6 exhibited almost smooth line at 15° and 22° implying depolymerization of α-cellulose occurred which results in increase in amorphous phase. This explains the IR spectrum of CG composite in Figure 1 where the peak absorption intensity which corresponded to C-H and C-O stretching vibrations at 2960, 2933, 2874, 1163 and 1032 cm^{-1} weaken caused by rupture and dehydration of α-cellulose (Ye et al. 2016). The depolymerization reaction of cellulose is shown in Figure 5. Apparently, dehydration and rupture of cellulose in CG composite caused it to demonstrate higher conductivity.

Conclusion

CG composite with high conductivity was successfully prepared using an eco-friendly method where no harmful chemicals or extreme high temperatures are used in the sol-gel method. BmimCl ionic liquid is favorable in dissolving α-cellulose and aided graphene dispersion. Increase in graphene content has increased the conductivity of CG composite provided that graphene is uniformly dispersed in cellulose matrix. This research provided an eco-friendly method to prepare cellulose/graphene composite which is useful in the energy field for future applications.

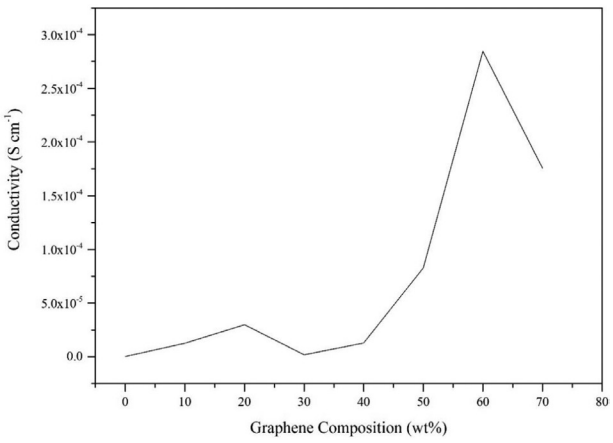

FIGURE 3. Conductivity of CG composite with different graphene composition

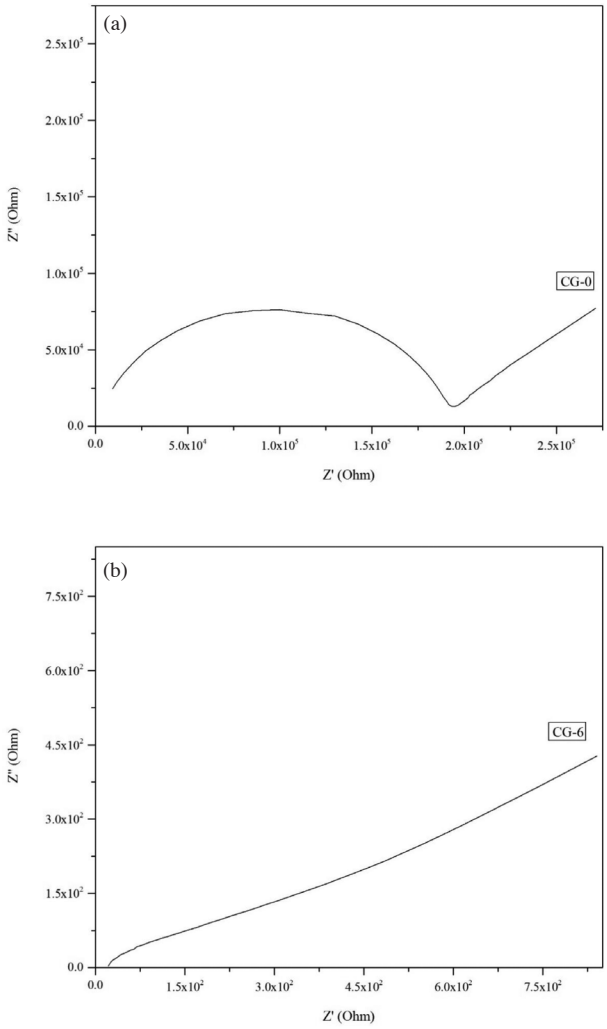

FIGURE 4. Nyquist plot of (a) CG-0 and (b) CG-6

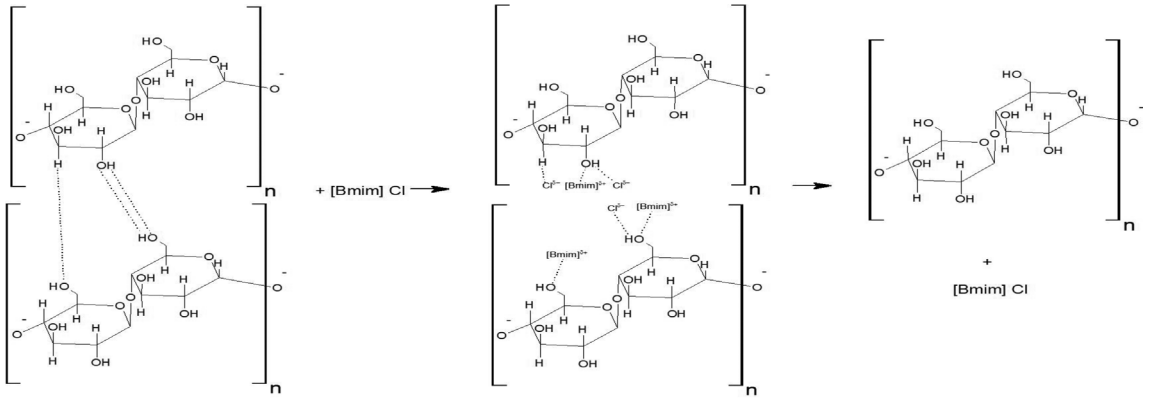

FIGURE 5. Depolymerization reaction of cellulose

ACKNOWLEDGEMENTS

This research is supported by the University of Malaya, Malaysia through Research Fund Assistance Grant (BK037-2015) and PPP Grant (PG220-2016A).

REFERENCES

Bag, S., Samanta, A., Bhunia, P. & Raj, C.R. 2016. Rational functionalization of reduced graphene oxide with imidazolium-based ionic liquid for supercapacitor application. *International Journal of Hydrogen Energy* 41(47): 22134-22143. doi: 10.1016/j.ijhydene.2016.08.041.

Bhaumik, P. & Dhepe, P.L. 2015. Conversion of biomass into sugars. In *Biomass Sugars for Non-Fuel Applications,* edited by Dmitry, M. & Olga, S. Pune, India: Royal Society of Chemistry. pp. 1-53. doi: 10.1039/9781782622079-00001.

Castro Neto, A.H., Guinea, F., Peres, N.M.R., Novoselov, K.S. & Geim, A.K. 2009. The electronic properties of graphene. *Reviews of Modern Physics* 81(1): 109-162. doi: 10.1103/RevModPhys.81.109.

Changgu, L., Xiaoding, W., Jeffrey, W.K. & James, H. 2008. Measurement of elastic properties and intrinsic strength of monolayer graphene. *Danish National Research Foundation* 321: 385-388. doi: 10.1126/science.1156211.

Feng, Y.Y., Zhang, X.Q., Shen, Y.T., Yoshino, K. & Feng, W. 2012. A mechanically strong, flexible and conductive film based on bacterial cellulose/graphene nanocomposite. *Carbohydrate Polymers* 87(1): 644-649. doi: 10.1016/j.carbpol.2011.08.039.

Hossain, M.M., Hahn, J.R. & Ku, B.C. 2014. Synthesis of highly dispersed and conductive graphene sheets by exfoliation of preheated graphite in a sealed bath and its applications to polyimide nanocomposites. *Buletin of the Korean Chemical Society* 35(7): 2049-2056. doi: 10.5012/bkcs.2014.35.7.2049.

Lavoinea, N., Guillard, V., Deslogesa, I., Gontard, N. & Brasa, J. 2016. Active bio-based food-packaging: Diffusion and release of activesubstances through and from cellulose nanofiber coating towardfood-packaging design. *Carbohydrate Polymers* 149: 40-50. doi: 10.1016/j.carbpol.2016.04.048.

Li, J., Cui, J., Yang, J., Ma, Y., Qiu, H. & Yang, J. 2016. Silanized graphene oxide reinforced organofunctional silane composite coatings for corrosion protection. *Progress in Organic Coatings* 99: 443-451. doi: 10.1016/j.porgcoat.2016.07.008.

Mahmood, N., Zhang, C., Yin, H. & Hou, Y. 2014. Graphene-based nanocomposites for energy storage and conversion in lithium batteries, supercapacitors and fuel cells. *Journal of Material Chemistry A* 2(1): 15-32. doi: 10.1039/c3ta13033a.

Pang, J., Liu, X., Zhang, X., Wu, Y. & Sun, R. 2013. Fabrication of cellulose film with enhanced mechanical properties in ionic liquid 1-allyl-3-methylimidaxolium chloride (AmimCl). *Materials* 6(4): 1270-1284. doi: 10.3390/ma6041270.

Patel, M.U.M., Luong, N.D., Seppala, J., Tchernychova, E. & Dominko, R. 2014. Low surface area graphene/cellulose composite as a host matrix for lithium sulphur batteries. *Journal of Power Sources* 254: 55-61. doi: http://dx.doi.org/10.1016/j.jpowsour.2013.12.081.

Qu, M., Yao, Y., He, J., Ma, X., Liu, S., Feng, J. & Hou, L. 2016. Tribological performance of functionalized ionic liquid and Cu microparticles as lubricating additives in sunflower seed oil. *Tribology International* 104: 166-174. doi: 10.1016/j.triboint.2016.08.035.

Sadasivuni, K.K., Ponnamma, D., Ko, H.U., Kim, H.C., Zhai, L. & Kim, J. 2016. Flexible NO2 sensors from renewable cellulose nanocrystals/iron oxide composites. *Sensors and Actuators B: Chemical* 233: 633-638. doi: 10.1016/j.snb.2016.04.134.

Safa, M., Chamaani, A., Chawla, N. & El-Zahab, B. 2016. Polymeric ionic liquid gel electrolyte for room temperature lithium battery applications. *Electrochimica Acta* 213: 587-593. doi: 10.1016/j.electacta.2016.07.118.

Singh, B.N., Panda, N.N., Mund, R. & Pramanik, K. 2016. Carboxymethyl cellulose enables silk fibroin nanofibrous scaffold with enhanced biomimetic potential for bone tissue engineering application. *Carbohydrate Polymers* 151: 335-347. doi: 10.1016/j.carbpol.2016.05.088.

Soheilmoghaddam, M., Pasbakhsh, P., Wahit, M.U., Bidsorkhi, H.C., Pour, R.H., Whye, W.T., & De Silva, R.T. 2014. Regenerated cellulose nanocomposites reinforced with exfoliated graphite nanosheets using BMIMCL ionic liquid. *Polymer* 55(14): 3130-3138. doi: 10.1016/j.polymer.2014.05.021.

Tian, M.W., Qu, L.J., Zhang, X.S., Zhang, K., Zhu, S.F., Guo, X.Q., Han, G.T., Tang, X.N. & Sun, Y.N. 2014. Enhanced mechanical and thermal properties of regenerated cellulose/graphene composite fibers. *Carbohydrate Polymers* 111: 456-462. doi: 10.1016/j.carbpol.2014.05.016.

Troter, D.Z., Todorovic, Z.B., Dokic-Stojanovic, D.R., Stamenkovic, O.S. & Veljkovic, V.B. 2016. Application of ionic liquids and deep eutectic solvents in biodiesel

production: A review. *Renewable and Sustainable Energy Reviews* 61: 473-500. doi: 10.1016/j.rser.2016.04.011.

Xu, M., Huang, Q., Wang, X. & Sun, R. 2015. Highly tough cellulose/graphene composite hydrogels prepared from ionic liquids. *Industrial Crops and Products* 70: 56-63. doi: http://dx.doi.org/10.1016/j.indcrop.2015.03.004.

Ye, W., Li, X., Zhu, H., Wang, X., Wang, S., Wang, H. & Sun, R. 2016. Green fabrication of cellulose/graphene composite in ionic liquid and its electrochemical and photothermal properties. *Chemical Engineering Journal* 299: 45-55. doi: http://dx.doi.org/10.1016/j.cej.2016.04.030.

Zhang, D.Y., Ge, C.W., Wang, J.Z., Zhang, T.F., Wu, Y.C. & Liang, F.X. 2016. Single-layer graphene-TiO2 nanotubes array heterojunction for ultraviolet photodetector application. *Applied Surface Science* 387: 1162-1168. doi: 10.1016/j.apsusc.2016.07.041.

Zhao, Y., Li, X.G., Zhou, X. & Zhang, Y.N. 2016. Review on the graphene based optical fiber chemical and biological sensors. *Sensors and Actuators B: Chemical* 231: 324-340. doi: 10.1016/j.snb.2016.03.026.

Farzana Abd Hamid & Fauzani Md. Salleh*
Chemistry Division
Centre for Foundation Studies in Science
University of Malaya
50603 Kuala Lumpur, Federal Territory
Malaysia

Nor Sabirin Mohamed & Syed Bahari Ramadzan Syed Adnan
Physic Division
Centre for Foundation Studies in Science
University of Malaya
50603 Kuala Lumpur, Federal Territory
Malaysia

*Corresponding author; email: alya5288@um.edu.my

Received: 18 October 2016
Accepted: 17 February 2017